Towards a virtual reality prototype for fuel cells

Beale, Steven; Jerome, Ronald; Ginolin, Anne; Perry, Martin; Ghosh, Dave

Publisher's version / Version de l'éditeur:

Phoenics Journal of Computational Fluid Dynamics and its Applications, 13, October 3, pp. 287-295, 2000

NRC Publications Record / Notice d'Archives des publications de CNRC:
https://nrc-publications.canada.ca/eng/view/object/?id=beca305d-8fdb-48f4-ba13-277cce64b895
https://publications-cnrc.canada.ca/fra/voir/objet/?id=beca305d-8fdb-48f4-ba13-277cce64b895

TOWARDS A VIRTUAL REALITY PROTOTYPE FOR FUEL CELLS

Steven Beale, Ron Jerome
National Research Council,
Ottawa, Ontario, Canada

Anne Ginolin
Institut Catholique d'Arts et Métiers,
Toulouse, France

Martin Perry, Dave Ghosh
Global Thermoelectric Inc.
Calgary, Alberta, Canada

May 1999

This work was conducted on Pentium PC operating under MSWindowsNT using PHOENICS version 3.2

Abstract:

The results of flow field simulations, in the manifolds and the passages of stacks of fuel cells, are presented. Detailed numerical simulations obtained using fine three-dimensional meshes are compared with results obtained using a simplified model based upon a distributed resistance analogy. It is shown that the latter may readily be used for engineering purposes. The geometry of the equipment is quite simple, however the flow fields, especially in the inlet manifold are complex. To this end, the use of a Virtual Reality facility to display the results proved beneficial. The flow-field calculations were used to re-design the equipment for improved uniformity of pressure and flow.

Introduction

Fuel cells are devices which convert chemical energy into electrical energy and heat (Appleby and Foulkes, 1989, Kordesh and Simader, 1996). They have a number of potential applications; for example as a replacement for combustion engines in automotive vehicles. In this context, the National Fuel Cells Initiative was recently undertaken as a strategic initiative by the National Research Council of Canada[1] as part of Canada's commitment to reduce greenhouse following the Kyoto summit.

There are three main parts to a fuel cell: Anode, cathode and electrolyte. The fuel, e.g. hydrogen, is fed into the anode and oxygen or air, is supplied via the cathode. Oxygen ions are transported through the solid oxide electrolyte, reacting with hydrogen at the anode. The flowing electrons provide a utilisable current. The exothermic reaction heats the fuel cell to an operating temperature of up to 1 000°C. Solid Oxide Fuel Cells[2] (SOFC's) offer a potential advantage in that methane or natural gas may used as the fuel. SOFC's are typically operated in stacks of ten or more. The configuration is similar to a single-pass cross-flow heat exchanger. Heat management is an important matter for concern: If the cell temperature is too low the chemical reaction will shutdown, while if it is too high mechanical failure of the system may occur; If just one cell in a stack fails, the entire stack is rendered useless. It is essential that the supply of air and fuel to each cell be uniform in order that the chemical reaction rate is the same at every cell in the stack, and thus the temperature distribution uniform.

Both air and fuel are being depleted within the passages of each cell assembly as a result of the chemical reaction, however it was ascertained that for a first analysis, the flow field would be analysed as a conservative field, in the absence of sinks due to chemistry, and with heat and mass transfer effects also neglected. The solution to this simpler design problem is prerequisite to progress when the latter effects are included, and provides a useful knowledge-base on which to develop more sophisticated tools in the future. A single-cell fuel cell model; into and out of a single multi-plate assembly, as well as a fuel cell stack model; within the inlet and exit headers (riser and downcomer) of the array of an entire stack assembly were therefore developed.

Mathematical Details

The problem to be solved is a steady three-dimensional (3-D) flow with air and/or methane as working fluids. These fluids are presumed to have constant properties. Two distinct approaches were considered.

(1) A direct numerical simulation (DNS) of the entire SOFC stack assembly, by means of the construction of a grid which is, not only large enough to cover the entire fuel-cell stack, but also fine enough to capture the detailed motion within the passages of each cell. While 10 years ago, a DNS approach would have been inconceivable, due to limitations of memory and speed, this is no longer the case. However such simulations still require very large calculation times, and result in the creation of very large data sets.

(2) For this reason a second approach based on a distributed resistance analogy (DRA) was developed. Fine-scale simulations are conducted within the inlet and exit manifolds, however the SOFC core is treated as if it were a porous media using local volume averaging with a distributed resistance, F, defined (Patankar and Spalding, 1972) as,

$$\vec{\nabla} p = F\vec{U} \tag{1}$$

where the 'filter' or 'superficial' velocity, $\vec{U}$, is given by,

$$\vec{U} = r\vec{u} \tag{2}$$

and $\vec{u}$ is a 'pore' or 'interstitial' velocity, and r the volume fraction of the working fluid. Inertial effects may be introduced, for example, as,

$$\frac{\partial(r_i\rho_i)}{\partial t}+\vec{\nabla}\cdot(r_i\rho_i\vec{u}_i)=0 \tag{3}$$

$$\frac{\partial(\rho_i r_i\vec{u}_i)}{\partial t}+\vec{\nabla}\cdot(\rho_i r_i\vec{u}_i;\vec{u}_i)=-r_i\vec{\nabla}p_i-Fr_i^2\vec{u}_i \tag{4}$$

Various other forms are also possible. The resistance term, F, may be evaluated; (i) using an analytical solution, (ii) experimentally from data of friction coefficient, f, vs. Reynolds' number, or (iii) from the results of detailed fine-scale numerical calculations for flow in 'typical' passages. The former (i) was employed here. For many fully-developed laminar duct flows,

$$f=\frac{a}{\mathrm{Re}} \tag{5}$$

with Re based on a hydraulic diameter[1], D_h,

$$\mathrm{Re}=\frac{D_h\rho u}{\mu} \tag{6}$$

Under these circumstances, it can be shown that,

$$F=\frac{2a}{r}\frac{\mu}{D_h^2} \tag{7}$$

The Appendix contains an analysis appropriate for plane ducts, see Kays and Crawford, 1966, for values of a and f for other cross-sections, obtained using numerical integration.

PHOENICS settings

The PHOENICS[3] code was used to performing all the flow calculations described in this paper. The OpenGL™-based virtual-reality (VR) editor, Ludwig and Spalding, 1999, was readily employed to set up the problem in an object-oriented (i.e. grid-independent) manner, and allowed for the prescription of the SOFC stack geometry and material properties, to be implemented with relative ease using the Arbitrary Solids Allocations Procedure (ASAP). For the DRA, the viscous-diffusion terms were turned off using group 12 patches (GP12DFE etc.) and the distributed resistance introduced with a patch type PHASEM and coefficient $C = rF/\rho$. After defining the geometry, mesh size, stored and solved-for variables, boundary conditions, numerical-control features etc., using the VR front-end, the actual flow calculations were performed using EARTH. The results were then displayed, as described below.

[1] Some authors introduce a hydraulic 'radius', $r_h = D_h/4$. This is not logical, however, since for a circular pipe the radius is $D_h/2$. According to Kays, 1996, usage appears to have propagated from the early text by McAdams, 1942.

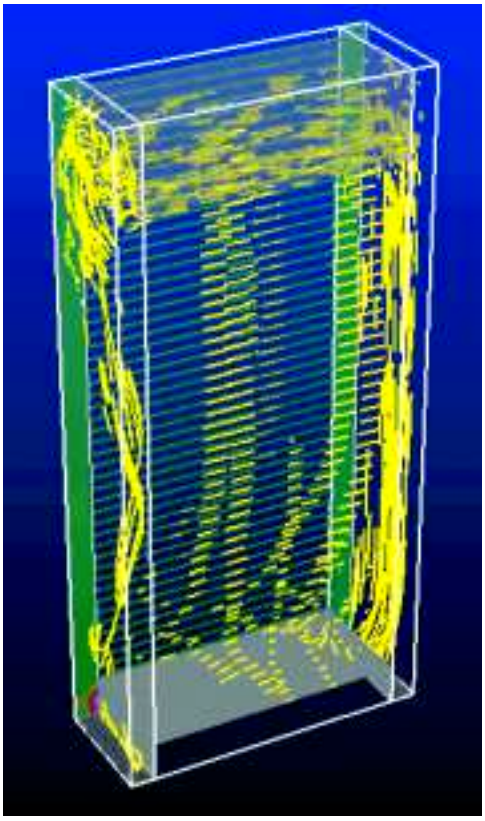

Figure 1. Particle traces constructed using visualisation software.

Figure 2. Observing the results in the VR facility.

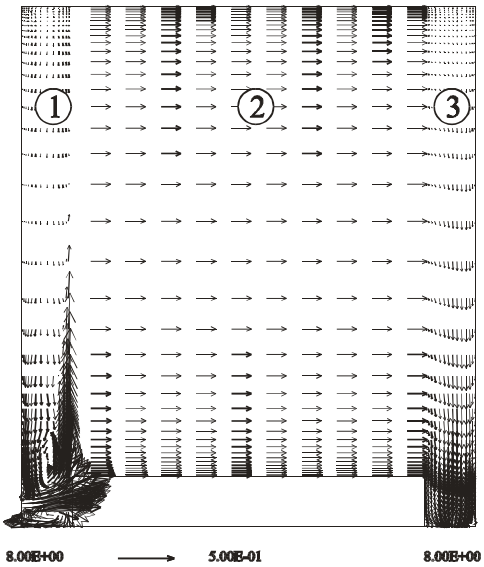

Figure 3. Velocity (m/s) in (1) Inlet manifold, (2) SOFC stack (3) Outlet manifold.

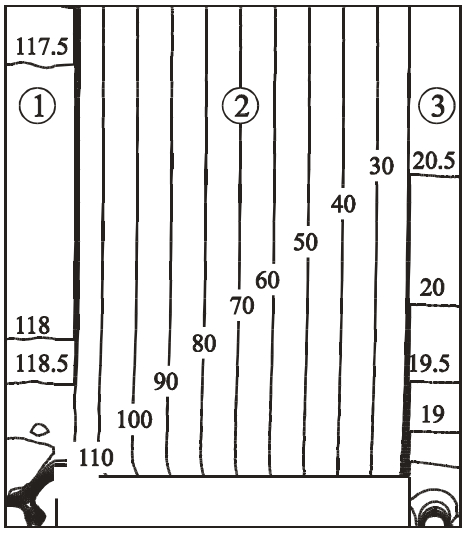

Figure 4. Pressure (Pa) in a SOFC stack and manifolds.

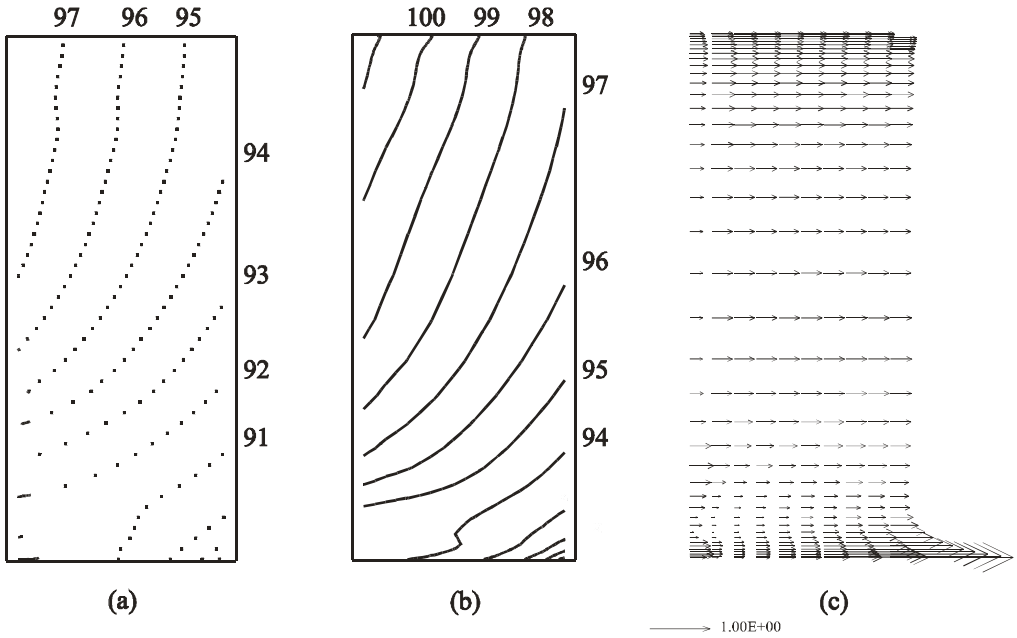

Figure 5**.** Pressure (Pa) contours in stack (a) DNS (b) DRA method; (c) Velocity (m/s) vectors DRA method.

Presentation of results

The NASA Flow Analysis Software Toolkit[4] (FAST), Walatka et al., 1992, and the Visual Toolkit[5] (VTK), Schroeder et al., 1997, were used for visualisation and animation. Immersion techniques were employed to render the results, in stereo, on a virtual reality (VR) wall. This environment consisted of a 10' by 8' screen, rear projection system, two-processor Silicon Graphics Onyx2 machine with a graphic pipe; and stereo glasses. In addition display of 3-D plots of vector and scalar fields in Virtual Reality Markup Language (VRML) allowed for the simultaneous viewing of results in Ottawa and Calgary via a secure web site. MPEG files of the animated sequences, observed on the VR wall were also constructed for display on personal computers. Figure 1 is an image of one such sequence, while Fig. 2 shows scientists observing the results of the work in the immersive environment.

Calculations were performed for single cells, 10-cell and 50-cell stacks. For the latter, the inlet is located in the side of the manifold, whereas the outlet is located in the bottom of the exit manifold. Figures 3 and 4 show velocity and pressure distributions, obtained using a DRA, on a vertical plane-of-symmetry. Note that for Fig. 3, the vector scale in the SOFC stack is different than that in the manifolds, owing to the larger differences in bulk velocity in these regions. It can be seen that the pressure distribution and hence the flow is quite uniform across the central core of the stack, in spite of the complex nature of the flow within the inlet manifold. A step is situated at the bottom of the stack-core, as a design requirement. Parametric studies were conducted to ascertain the influence of various geometric parameters; channel height, H, pitch, P, width, b (see the Appendix).

Figures 5(a) and 5(b) show pressure distributions obtained using DNS and DRA methods in the stack core for a second SOFC design. It can be seen that agreement between the two methods is good. Inspection of the pressure contours and velocity vectors, Fig. 5(c), reveal that for this design, flow uniformity is far from satisfactory in comparison to the results of Figs. 3 and 4.

Convergence and grid independence

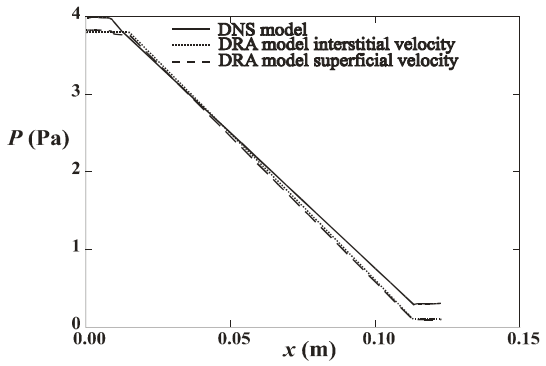

Figure 6: Pressure (Pa) vs. x (m), for three methods used in a 10-cell model.

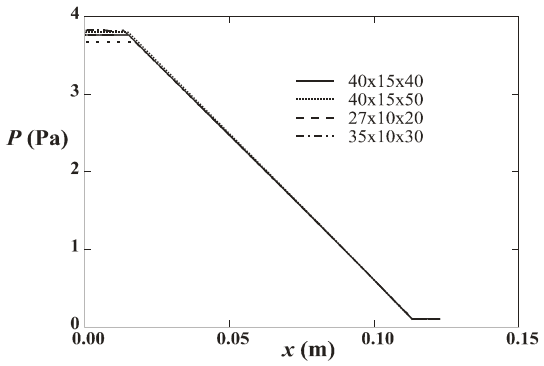

Figure 7: Pressure (Pa) vs. x (m), for three four different meshes

Calculations were performed to assess the measure of grid independence achieved for the results of this study, i.e. to quantify the impact of the number of mesh points upon the solution. Four different sizes were considered, using the DRA method. These are illustrated below in Fig. 7. It can be seen that a reasonable independence of the pressure distribution from the grid size has been realized for the problem under consideration.

Computer storage and time

For the DNS results presented in Fig. 5(a); Total required F-array storage was 1.7×10^6 elements. A total of 3000 sweeps were employed over a total of 8.7×10^3 sec. (2.4 hours). Convergence was achieved after approximately 50% elapsed time . For the DRA method used to generate the results of Fig. 5(b), required F-array storage was 11.3×10^6 elements. Two thousand (2000) sweeps were performed over a total of 44.8×10^3 sec. (12.4 hours). Convergence was achieved near to the end of the run.

Discussion of results

Physical realism and numerical accuracy

Figure 3 shows vectors in (1) the inlet manifold, (2) the stack-core and (3) the outlet manifold. Although the geometry is quite simple, the flow regime within the inlet manifold is complex; the initially horizontal influent impinges on the step at the base of the assembly and then diverges in various directions in 3-D. Flow on the core-side of the inlet manifold is channel-like with downflow occurring in the upper regions. In spite of this, flow within the passages of the SOFC stack is quite uniform, suggesting the design to be a good one. Note there is little variation in the vectors across the core, in spite of the complex re-circulating 3-D flow in the manifold: Because the core-flow is a low Reynolds number or creeping flow, it is the pressure gradient which drives the flow; inertial or convective influences are subordinate. Flow in the outlet manifold is less complex than that in the inlet; due to the upwind nature of convection; and the size and form of the fluid outlet is less critical than is the case for the inlet.

Figure 4 shows isobars on the vertical symmetry plane. A pressure maximum occurs at the point-of-impingement at the step. The pressure gradient across the stack (2) is quite uniform in the horizontal direction. In the manifolds (1),(3) the gradient is relatively small and decreases with height, due to injection/suction of matter into and out of the SOFC stack. The mean pressure difference across the stack-core was computed both from the

data and from Eq. (10) assuming fully-developed uniform flow. In most cases, the mean pressure drop across the stack approaches theoretical values, i.e., local variations in velocity and pressure average out. The pressure difference between the inlet and outlet, $\Delta P_{\text{overall}}=\Delta P_{\text{stack}}+\Delta P_{\text{manifolds}}$, was also computed as a measure of the required pumping power. Manifold losses are in many cases quite significant, with substantial variations being observed, depending on the particular configuration under consideration. For uniform flow the ratio of $\Delta P_{\text{stack}}/\Delta P_{\text{manifolds}}$ should be large. The results of the parametric studies, revealed which of the geometric parameters were important and allowed for the stack design to be optimised.

Comparison of DNS and DRA methods

Figure 5 is a comparison of a DNS approach with a DRA approach based on Eqs. (3)-(4). The dashed lines in Fig. 5(a) are due to the pressure not being defined in solid regions. It can be seen that the DRA and DNS results are similar with small systematic differences in the absolute values being observed: From Eq. (10), the slope of the pressure gradient, dP/dx is proportional to $1/H^3$, for constant $\vec{U}$, so the deviations are rather minor. The details of the velocity profile in the DNS model are, of course, lost with the DRA.

For the results of Fig. 5, the core resistance is small, and inertial effects cannot be excluded: The pressure and velocity distributions are less uniform than for the previous case. Figure 5(c) also shows velocity vectors across the SOFC core for this case. The flow fields tend to be fairly uniform over the central region of the core, with increased magnitude towards the bottom of the stack, and decreased values towards the top. For a large stack it is necessary to maintain sufficiently high viscous losses, and associated pressure gradient within the core, so that the inertial effect associated with suction and injection of the working fluid out of and into the two manifolds, does not lead to fuel starvation at the top of the core.

In Eq. (4), the 'convecting' terms are components of the superficial velocity, $\vec{U} = r\vec{u}$, but the 'convected' terms (dependent variables) are components of the interstitial velocity. It is also possible to construct DRA approaches, where the solid regions are blocked and the interstitial velocity $\vec{u}$ alone is present or where the superficial velocity, $\vec{U}$, is treated as both the convecting and convected terms, obviating the additional storage requirements for the porosities. Figure 6 shows a comparison for the latter two cases; in general only minor differences occur when inertia is small. An approach based on an the interstitial velocity $\vec{u}$, is always equivalent to Equations (3)-(4), however the $\vec{U}$-based method is strictly so if and only if the influence of convection is negligibly small. Where inertia effects are significant, the recommended approach is that of Eqs. (3)-(4), since a coarse grid, whose elements need not necessarily coincide with the interfaces between the fuel-cell interconnect devices, and the passages within which the working fluid flows, may readily be employed. It must be admitted that this is a subjective position, since in all cases, a closure assumption has been invoked, the best solution being therefore the simplest for the task at hand. The DRA approach is a reasonable facsimile for DNS, and may be considered as providing a balance between simple lumped-capacity hydrodynamic models, which are over-simplistic, and DNS calculations which are overly time-consuming, at present.

Significance in relation to objective of work

Numerical calculations of fluid flow within the various stacks of design prototypes suggested that certain models were superior. Salient features of the flow field were identified, and design improvements effected. For flow in large SOFC stacks, the back pressure across the stack assembly should be significantly larger than the hydraulic resistance in the inlet manifold in order to maintain uniformity of pressure and velocity across the core.

The geometric features, by which this may be achieved were identified using parametric studies, and the SOFC design re-configured for uniformity, as a result of this CFD study.

Conclusions

A DRA model was used as an engineering tool to assist in the design of SOFC's using CFD, with a measure of confidence: Certain details of the flow field, such as the periodic viscous effects of the cells on the flow in the manifolds are suppressed with the DRA. However, as a basic tool, the DRA combines computational speed with reasonable accuracy, and is an acceptable method for modelling SOFC's because of the associated economies of computer run-time and memory.

Recommendations

Research is now being conducted into SOFC's with planar and more complex passages. The flow of both working fluids, combined with inter-fluid heat transfer and Ohmic heating is being considered. Concurrent (interactive) display and manipulation of graphics data, locally on VR walls, and across the country via the high-speed internet[6] CA*net 3 is also the subject for research. Experimental facilities are being built to gather empirical data and conduct flow visualisation studies for model validation purposes.

Acknowledgement

Financial support for this project was provided by Global Thermoelectric Inc., the Institute for Chemical Process and Environmental Technology, and the Environmental Management Office of the National Research Council. The authors wish to thank Dr. Pierre Boulanger of NRC's Institute for Information Technology for providing access to the VR facility, and to Dr. John Ludwig at CHAM for technical support.

Appendix: Plane duct geometry

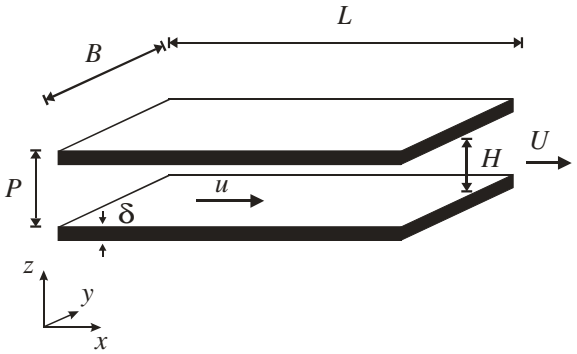

Figure 8. Schematic of a plane duct.

For fully-developed flow between parallel plates, Langlois, 1964, with $r = H/P$, it can readily be shown that the friction coefficient is given by,

$$f = \frac{\tau_w}{\frac{1}{2}\rho u^2} = \frac{12\mu}{\rho H u} \tag{8}$$

and the distributed resistance is obtained as,

$$F = \frac{12P\mu}{H^3} \tag{9}$$

In the z direction the velocity is presumed zero, $w = 0$. The pressure drop across the stack is just,

$$\Delta\overline{p} = \frac{12L\mu u}{H^2} = \frac{12L\mu\dot{Q}}{nBH^3} \tag{10}$$

where n is the number of cells in the stack, B is the width of the duct in the y-direction and $\dot{Q} = nBHu$ is the prescribed volumetric discharge, assuming uniform flow conditions.

Literature references

Appleby, A.J., and Foulkes, F.R. *Fuel Cell Handbook*, Van Nostrand Reinhold, New York, 1989.
Globus, A., Levit, C. Lasinski, T. A Tool for Visualizing the Topology of Three-dimensional Vector Fields. Report RNR-91-017. NASA Ames Research Center, Moffett Field, CA, 1991.
Heat Exchanger Design Handbook, Vol. 1. Heat Exchanger Theory, *Ed.* Hewitt, G.F., et. al, Hemisphere, Washington, 1983. pp. 1.2.6-1 - 1.2.6-7.
Kays, W.M. Personal Communication, 1996.
Kays, W.M. and Crawford, M.E. *Convective Heat and Mass Transfer,* 2nd ed., McGraw-Hill, New York, 1966.
Kordesh, K., and Simader, G. *Fuel Cells and their Applications*, John Wiley, New York, 1996.
Langlois, W.E. *Slow Viscous Flow*, MacMillan, London, 1964.
Ludwig, J.C. and Spalding, D.B. PHOENICS-VR Reference Guide, Version 3.2, TR326. CHAM Ltd., 1999.
McAdams, W.H. *Heat transmission*, 2nd ed. McGraw-Hill, New York, 1942.
Patankar, S.V., *Numerical heat transfer and fluid flow*, Hemisphere, Washington, 1980.
Patankar, S.V., and Spalding, D.B. A Calculation Procedure for the Transient and Steady-state Behaviour of Shell-and-tube Heat Exchangers, TR EF/TN/A/48, Imperial College of Science and Technology, London, 1972.
Schroeder, W., Martin, K., and Lorensen, W. *The Visualisation Toolkit*, 2nd ed. Prentice Hall, Upper Saddle River, 1997.
Walatka, P.P., Clucas, J., McCabe, R.K. and Plessel, T. *FAST User Guide.* RND-92-013. NASA. 1992.

Non-standard nomenclature

B	Width
F	Distributed resistance
k	Permeability
L	Length of core assembly
$\vec{U}$	Superficial velocity
$\vec{u}$	Interstitial velocity
H	Height
N	Number of cells in stack
P	Pitch
$\dot{Q}$	Volumetric discharge
δ	Thickness

Useful web sites

[1] NRC web site: http://www.nrc.ca
[2] Global Thermoelectric web site: http://www.globalte.com
[3] CHAM web site: http://www.cham.co.uk
[4] NASA FAST web site: http://science.nas.nasa.gov/Software/FAST/
[5] The Visualization Toolkit web site: http://www.kitware.com/vtk.html
[6] CANARIE web site: http://www.canarie.ca/